Numerical Simulations of Flow in Axial Compressor System, Preparatory Steps for Active Control

Irina-Carmen ANDREI[1], Gabriela STROE*,[2]

*Corresponding author
[1]INCAS – National Institute for Aerospace Research "Elie Carafoli",
B-dul Iuliu Maniu 220, Bucharest 061126, Romania,
andrei.irina@incas.ro, icandrei28178@gmail.com
[2]"POLITEHNICA" University of Bucharest, Faculty of Aerospace Engineering,
Gh. Polizu Street 1-7, Sector 1, Bucharest, 011061, Romania,
ing.stroe@yahoo.com*

DOI: 10.13111/2066-8201.2018.10.3.2

Received: 29 May 2018/ Accepted: 21 June 2018/ Published: September 2018

6th International Workshop on Numerical Modelling in Aerospace Sciences, NMAS 2018*,*
16 - 17 May 2018, Bucharest, Romania, (held at INCAS, B-dul Iuliu Maniu 220, sector 6)
Section 1 – Launchers propulsion technologies and simulations of rocket engines

Abstract: *For most compressor flows, the existence of turbulent shear stresses is essential to compensate and overcome the adverse pressure gradients without separation. The performance of compressor improves as the turbulent stresses get stronger relative to the laminar viscous stresses, which become significant as the Reynolds number increases. The methods used to design subsonic axial flow compressors and fans are based on correlations such as deviation angle vs. incidence angle to obtain the expected performance for a particular blade profile. In this paper, compressor models that are used frequently in controller designs are described and the effect of the assumptions on the prediction capability of these models is explained. The control concepts used to maintain and therefore grant the stable operation are presented and monitored, as well as an outline of sensors, actuators and automatic controllers is given. The survey concludes that the behavior of a compressor system subsequent to instability onset is reasonably understood but the considered models can not describe all types of instabilities encountered. There comes the recommendation that for a better understanding of the mechanisms behind the onset of such instabilities, refinements as new improvements of the existing models are require, which may give insights into new automatic control methods.*

Key Words: *Automatic control, axial compressor system, controller, instabilities*

1. INTRODUCTION

The axial compressors have a large variety of applications in aircraft industry; they represent a basic component of the jet engines (turbojet, turbofan, turboprop and turboshaft engines), which are supposed to perform for aerospace propulsion, industrial gas turbines that generate high power output, and processors targeted to pressurize gas or fluids, with applications to chemical phenomena. [9] The axial compressors can maneuver a higher mass flow rate for the same frontal cross section. This particular reason, in conjunction with the fact that the

thrust of the engine is highly increased due to the significant enlargement of the compressor pressure ratio and air mass flow rate, are the important justifications for the use large scale use of the axial compressors in aircraft jet engines [9].

For most type of the jet engines, the compression system consists in fan, low-pressure compressor LPC and high-pressure compressor HPC. From the flow direction's standpoint, the fan is of axial flow-type, while the LPC and HPC can be of axial flow-type, centrifugal flow-type or both [9]. An axial compressor system consists in sequence of blade row cascades; usually, a compressor stage is made up from a rotating cascade and a fixed one [9]. The working fluid is passed through the fixed and rotating blades; the energy transfer is performed within the rotating blade row; the fluid flow is guided inside the fixed blade rows, and in certain cases, according to the cascade design, the fluid flow can be directed through the rotating blade rows [9]. The high-performance compression stages are transonic (most of them high subsonic to transonic), where regions of subsonic and supersonic flow both exist in the blade passages. The steady state performance of an axial compressor system is described by the universal map of the axial compressor, which plots the averaged mass flow rate versus the total pressure ratio; such diagram is also referred as the characteristic or performance map of the compressor.

2. COMPUTATIONAL STUDIES OF AXIAL COMPRESSOR SYSTEM

It is strongly recommended to avoid surge and rotating stall, because such phenomena can lead to mechanical and thermal loads and can cause significant structural damage of the aircraft engine parts. These aerodynamic instabilities are oscillating phenomena and can reduce the possibility to increase the pressure and may induce a severe decay of the compression system efficiency. There are three different methods to compensate for these problems, namely: surge or stall avoidance, surge detection and avoidance, and increasing the stall margin approach [3-7].

For the first method, the automatic control systems, does not allow the compressor to operate on the left side of the surge line. In order to locate the surge line on the compressor map, a safety margin is specified. This safety margin may be defined as a function of the pressure ratio, corrected mass flow or a numerical combination of pressure ratio and corrected mass flow. The safety margin noted SM, is defined as a function of total pressure ratio as [5-7]

$$SM = \frac{\left(\frac{P_{02}}{P_{01}}\right)_{Surge} - \left(\frac{P_{02}}{P_{01}}\right)_{Surge\ Avoidance}}{\left(\frac{P_{02}}{P_{01}}\right)_{Surge\ Avoidance}} \tag{1}$$

The total pressure at the compressor outlet and inlet is noted by P_{01} and P_{02}, respectively. In both case of control, active and passive, the characteristic performance maps of the axial compressor are modified and the surge line is shifted to a lower mass flow. An advantage of this methodology consists in the fact that the axial compressor can operate near the peak efficiency and high-pressure ratios at lower mass flow rates. In the case of the passive surge or stall, the geometry of the axial compressor is changed such that to modify the stall margin [9-10]. The use of the variable inlet guide vanes represents a good option for increasing the stall margin; it has been successfully used to control the stall in axial compressors. With this methodology, the incidence angle in axial compressors at lower mass flow rates is reduced and the leading-edge LE separation is avoided. Within the inlet guide

vanes, the direction of the flow at the leading edge is modified such that the angle of attack decreases. The variable inlet guide vanes are very often used while starting and accelerating the aircraft engines, in order to avoid the crossing of the surge line. In active stall or surge control, the axial compressor is equipped with devices, such as a bleed valve that can be switched in the positions on or off. The active surge or stall control may be classified into two classes: open-loop and closed-loop. In the case of closed-loop control, a feedback law is applied to activate the controller, while in the open-loop control there are no feedback signals [11-13].

Other methods used to avoid active surge or stall control, are represented by air injection, air bleeding, and recirculation (a mix of injection and bleeding) [11-13].

Air injection is a method in which small amount of high pressure and high velocity air is injected into the axial compressor upstream of the compressor inlet. This way, the flow and the axial velocity component are increased; also, the local angles of attack are reduced, and therefore, the leading-edge LE separation is compensated. The injected air may be obtained from the diffuser downstream of the axial compressor or from an auxiliary device [14-17].

Bleeding technique has been used to enable the efficient operation of the compressor system, for a wide range of operating conditions.

The bleed valve is usually located either in the plenum exit or downstream of rotor on the shroud. The bleeding system operation consists in introducing or expelling of a lower fluid mass flow rate, taken from the working fluid, which does not have enough momentum to overcome the viscous and adverse pressure gradient forces in the plenum. By removing a part of the highly pressurized flow downstream of the compressor, flow acceleration can increase and surge-free operation is obtained [14-17].

Closed-loop active control represents an important integral part of the aircraft engines, called the smart or intelligent aircraft engines. The closed-loop active control systems use a sensor for detecting the growth of instabilities when an axial compressor reaches the stall conditions. By applying this method, a control unit processes measured flow field data, the temperature, pressure or axial velocity, from a stall-detection system.

A feedback control law connecting the sensed fluctuations to the rate of bleed is used to stabilize the axial compressor. The control unit activates a set of actuator systems. Various types of actuators are used for stabilizing the axial compressor system, for example: bleed valve actuators, variable inlet guide vanes, recirculation, loudspeakers, movable plenum walls, and air injections [14-17].

One of the most important methods for investigating the complex flow phenomena in aircraft engines system is the Computational Fluid Dynamics - CFD.

For many applications, the flow regime can be considered incompressible, and the Laplace and Poisson equations can be applied to model the flow within the inlet and exit ducts, respectively [14-17]. The pressure field calculations are independent of viscous effects and can be calculated with mathematical classical models [18-20].

It is convenient to work with the full Navier-Stokes equations for mathematical modeling and to perform numerical simulations, purposed to study the off-design conditions by Computational Fluid Dynamics methods.

The Navier-Stokes equations describe the physical 3D model for the unsteady compressible viscous flow, with the assumptions of the perfect Newtonian fluids and the Stokes linear stress-strain rate low considered [4].

In 3D Cartesian coordinates, the conservative equations in vector form are written, and then for 3D unsteady compressible Reynolds-Averaged Navier-Stockes RANS equations are presented in integral form and calculated with a finite volume scheme [4].

$$\frac{\partial q}{\partial t}+\frac{\partial E}{\partial x}+\frac{\partial F}{\partial y}+\frac{\partial G}{\partial z}=\frac{\partial R}{\partial x}+\frac{\partial S}{\partial y}+\frac{\partial T}{\partial z} \tag{2}$$

$$q=\begin{Bmatrix}\rho\\ \rho u\\ \rho v\\ \rho w\\ E_t\end{Bmatrix}, E=\begin{Bmatrix}\rho u\\ \rho u^2+p\\ \rho uv\\ \rho uw\\ (E_t+p)u\end{Bmatrix}, F=\begin{Bmatrix}\rho v\\ \rho uv\\ \rho v^2+p\\ \rho vw\\ (E_t+p)v\end{Bmatrix}, G=\begin{Bmatrix}\rho w\\ \rho uw\\ \rho vw\\ \rho w^2+p\\ (E_t+p)w\end{Bmatrix} \tag{3}$$

$$E_t=\rho[C_vT+\frac{1}{2}(u^2+v^2+w^2)] \tag{4}$$

$$p=\rho RT \tag{5}$$

$$p=(\gamma-1)[E_t-\frac{1}{2}\rho(u^2+v^2+w^2)] \tag{6}$$

$$R=\begin{Bmatrix}0\\ \tau_{xx}\\ \tau_{xy}\\ \tau_{xz}\\ u\tau_{xx}+v\tau_{xy}+w\tau_{xz}+q_x\end{Bmatrix}, \qquad S=\begin{Bmatrix}0\\ \tau_{yx}\\ \tau_{yy}\\ \tau_{yz}\\ u\tau_{yx}+v\tau_{yy}+w\tau_{yz}+q_y\end{Bmatrix}, \tag{7}$$

$$T=\begin{Bmatrix}0\\ \tau_{zx}\\ \tau_{zy}\\ \tau_{zz}\\ u\tau_{zx}+v\tau_{zy}+w\tau_{zz}+q_z\end{Bmatrix} \tag{8}$$

$$\tau_{xx}=\lambda\left(u_x+v_y+w_z\right)+2\mu u_x \tag{9}$$

$$\tau_{xy}=\tau_{yx}=\mu(u_y+v_x) \tag{10}$$

$$\tau_{xz}=\tau_{zx}=\mu(u_z+w_x) \tag{11}$$

$$\tau_{yy}=\lambda\left(u_x+v_y+w_z\right)+2\mu u_y \tag{12}$$

$$\tau_{yz}=\tau_{zy}=\mu(v_z+w_y) \tag{13}$$

$$\tau_{zz}=\lambda\left(u_x+v_y+w_z\right)+2\mu u_z \tag{14}$$

$$q_x=-k\frac{\partial T}{\partial x} \tag{15}$$

$$q_y=-k\frac{\partial T}{\partial y} \tag{16}$$

$$q_z=-k\frac{\partial T}{\partial z} \tag{17}$$

$$p_{ref}=\frac{\rho_{ref}V_{ref}^2}{\gamma} \tag{18}$$

$$\iiint_V\frac{\partial q}{\partial t}dV+\iint_S(E\vec{\imath}+F\vec{\jmath}+G\vec{k})\vec{n}dS-\iint_S q\overrightarrow{V_G}\vec{n}dS=\iint_S(R\vec{\imath}+S\vec{\jmath}+T\vec{k})\vec{n}\,dS \tag{19}$$

$$\iint_S \left(E\vec{\imath} + F\vec{\jmath} + G\vec{k}\right)\vec{n}dS - \iint_S q\overrightarrow{V_G}\,\vec{n}dS =$$
$$= \sum_{All\ Faces} \left(En_x + Fn_y + Gn_z\right)\Delta S - \left[q\overrightarrow{V_G}\vec{n}\Delta S\right] = \tag{20}$$
$$= \left[\hat{E}_{i+\frac{1}{2},j,k} + \hat{E}_{i-\frac{1}{2},j,k}\right] + \left[\hat{F}_{i,j+\frac{1}{2},k} + \hat{F}_{i,j-\frac{1}{2},k}\right] + \left[\hat{G}_{i,j,k+\frac{1}{2}} + \hat{G}_{i,j,k-\frac{1}{2}}\right]$$

$$\hat{E}\Big|_{i\pm\frac{1}{2},j,k} = \left[En_x + Fn_y + Gn_z - q\left(\overrightarrow{V_G}\vec{n}\right)\right]\Delta S\Big|_{i\pm\frac{1}{2},j,k} \tag{21}$$

$$\hat{F}\Big|_{i,j\pm\frac{1}{2},k} = \left[En_x + Fn_y + Gn_z - q\left(\overrightarrow{V_G}\vec{n}\right)\right]\Delta S\Big|_{i,j\pm\frac{1}{2},k} \tag{22}$$

$$\hat{G}\Big|_{i,j,k\pm\frac{1}{2}} = \left[En_x + Fn_y + Gn_z - q\left(\overrightarrow{V_G}\vec{n}\right)\right]\Delta S\Big|_{i,j,k\pm\frac{1}{2}} \tag{23}$$

$$\iint_S (R\vec{\imath} + S\vec{\jmath} + T\vec{k})\vec{n}dS = \sum_{All\ Faces} (Rn_x + Sn_y + Tn_z)\Delta S \tag{24}$$

$$f_{Numerical} = \left[\overbrace{\frac{1}{2}[f(q_L) + f(q_R)]}^{Physical\ Flux\ Term} - \overbrace{\frac{1}{2}\left[\left|\tilde{A}(q_L, q_R)\right|(q_L - q_R)\right]}^{Artificial\ Viscosity\ Team}\right]\Delta S \tag{25}$$

$$f(q_L) = \begin{bmatrix} \rho_L U_L \\ \rho_L U_L u_L + p_L n_x \\ \rho_L U_L v_L + p_L n_y \\ \rho_L U_L w_L + p_L n_z \\ U_L H_{0L} - p_L n_t \end{bmatrix}, f(q_R) = \begin{bmatrix} \rho_R U_R \\ \rho_R U_R u_R + p_R n_x \\ \rho_R U_R v_R + p_R n_y \\ \rho_R U_R w_R + p_R n_z \\ U_R H_{0R} - p_R n_t \end{bmatrix} \tag{26}$$

$$q_L = \begin{bmatrix} \rho_L \\ u_L \\ v_L \\ w_L \\ p_L \end{bmatrix}, q_R = \begin{bmatrix} \rho_R \\ u_R \\ v_R \\ w_R \\ p_R \end{bmatrix} \tag{27}$$

$$U = (\vec{V} - \overrightarrow{V_G})\vec{n} \tag{28}$$

$$H_0 = E_t + p \tag{29}$$

$$n_t = -\overrightarrow{V_G}\vec{n} \tag{30}$$

$$q_L = q_i + \frac{1}{6}\Phi^+_{i-\frac{1}{2}}(q_i - q_{i-1}) + \frac{1}{3}\Phi^-_{i+\frac{1}{2}}(q_{i+1} - q_i) \tag{31}$$

$$q_R = q_{i+1} - \frac{1}{3}\Phi^+_{i+\frac{1}{2}}(q_{i+1} - q_i) - \frac{1}{6}\Phi^-_{i+\frac{3}{2}}(q_{i+2} - q_{i+1}) \tag{32}$$

$$\Phi^+_{i-\frac{1}{2}} = \Phi\left(r^+_{i-\frac{1}{2}}\right), \Phi^-_{i+\frac{1}{2}} = \Phi\left(r^-_{i+\frac{1}{2}}\right) \tag{33}$$

$$r^{+}_{i-\frac{1}{2}} = \frac{q_{i+1} - q_i}{q_i - q_{i-1}}, r^{-}_{i+\frac{1}{2}} = \frac{q_i - q_{i-1}}{q_{i+1} - q_i} \tag{34}$$

$$\Phi(r) = max[0, min(2r, 1), min(r, 2)] \tag{35}$$

$$\left|\tilde{A}(q_L, q_R)\right|(q_R - q_L) = \left|\widetilde{\lambda_1}\right|\Delta q + \delta_1\widetilde{q^*} + \delta_2 N_n \tag{36}$$

$$\delta_1 = \left(-\left|\widetilde{\lambda_1}\right| + \frac{\left|\widetilde{\lambda_2}\right| + \left|\widetilde{\lambda_3}\right|}{2}\right)\frac{\Delta p}{\widetilde{a^2}} + \frac{\left|\widetilde{\lambda_2}\right| - \left|\widetilde{\lambda_3}\right|}{2}\frac{\tilde{q}\Delta U}{\tilde{a}} \tag{37}$$

$$\delta_2 = \left(-\left|\widetilde{\lambda_1}\right| + \frac{\left|\widetilde{\lambda_2}\right| + \left|\widetilde{\lambda_3}\right|}{2}\right)\tilde{q}\Delta U + \frac{\left|\widetilde{\lambda_2}\right| - \left|\widetilde{\lambda_3}\right|}{2}\frac{\Delta p}{\tilde{a}} \tag{38}$$

$$\widetilde{q^*} = \begin{bmatrix} 1 \\ \tilde{u} \\ \tilde{v} \\ \widetilde{w} \\ \widetilde{H_0} \\ \tilde{\rho} \end{bmatrix}, N_n = \begin{bmatrix} 0 \\ n_x \\ n_y \\ n_z \\ \widetilde{U} \end{bmatrix}\Delta S \tag{39}$$

$$\widetilde{\lambda_1} = \widetilde{U} \tag{40}$$

$$\widetilde{\lambda_2} = \widetilde{U} + \tilde{a} \tag{41}$$

$$\widetilde{\lambda_3} = \widetilde{U} - \tilde{a} \tag{42}$$

$$\tilde{q} = \sqrt{\rho_L \rho_R} \tag{43}$$

$$\tilde{u} = \frac{\sqrt{\rho_L}u_L + \sqrt{\rho_R}u_R}{\sqrt{\rho_L} + \sqrt{\rho_R}} \tag{44}$$

$$\tilde{v} = \frac{\sqrt{\rho_L}v_L + \sqrt{\rho_R}v_R}{\sqrt{\rho_L} + \sqrt{\rho_R}} \tag{45}$$

$$\widetilde{w} = \frac{\sqrt{\rho_L}w_L + \sqrt{\rho_R}w_R}{\sqrt{\rho_L} + \sqrt{\rho_R}} \tag{46}$$

$$\widetilde{H} = \frac{\sqrt{\rho_L}H_L + \sqrt{\rho_R}H_R}{\sqrt{\rho_L} + \sqrt{\rho_R}} \tag{47}$$

$$\widetilde{U} = \left(\widetilde{u}\vec{\imath} + \tilde{v}\vec{\jmath} + \widetilde{w}\vec{k}\right)\vec{n} - \overrightarrow{V_G}\vec{n} \tag{48}$$

$$\Delta p = p_R - p_L \tag{49}$$

In the case of the experimental analysis carried on for studying the engine core flow, for many applications, the Reynolds number has large values and the flow regime is turbulent. Time and length scales of the turbulent flow regimes are very small. In order to apply the turbulent regime conditions directly from the Navier-Stokes equations, the grid resolution must be as high as possible [4].

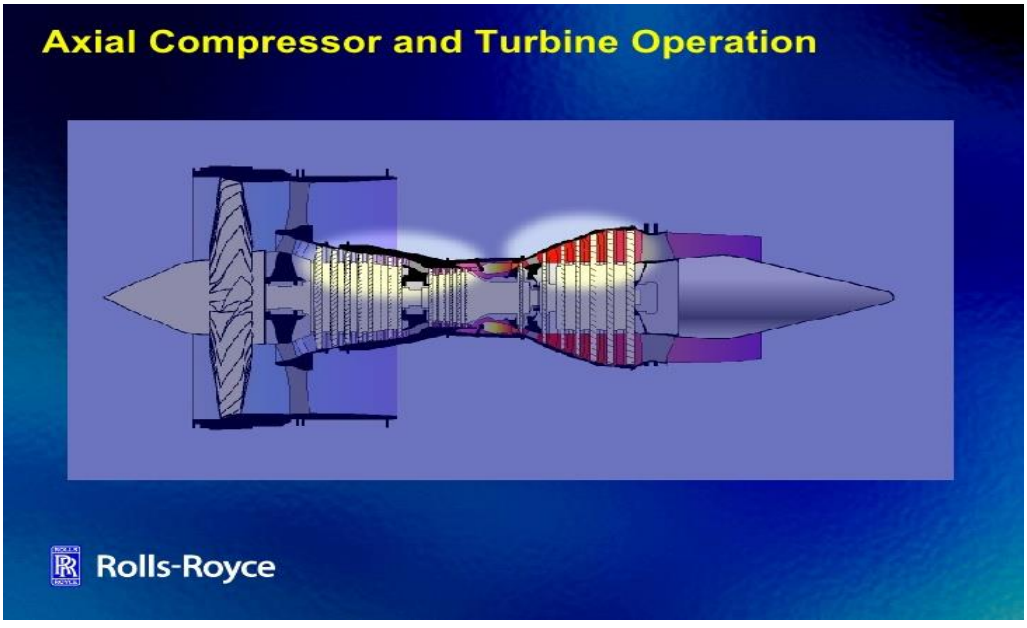

Fig. 1 - Schematic diagram of the turbofan engine, illustrating the Axial Compressor and Turbine Operation, Rolls-Royce [1]

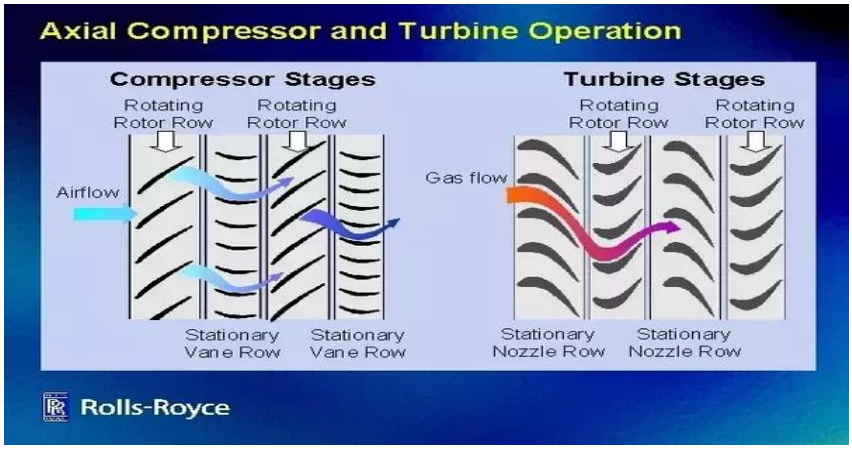

Fig. 2 - Schematic diagram of the compressor and turbine stages, turbofan engine, Rolls-Royce [1]

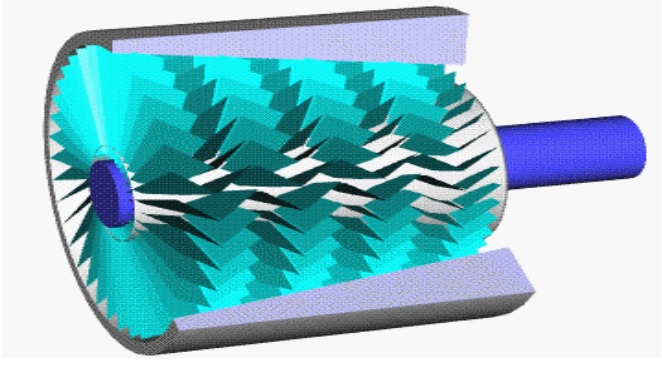

Fig. 3 - Schematic diagram of multiple-staged axial flow compressor [2]

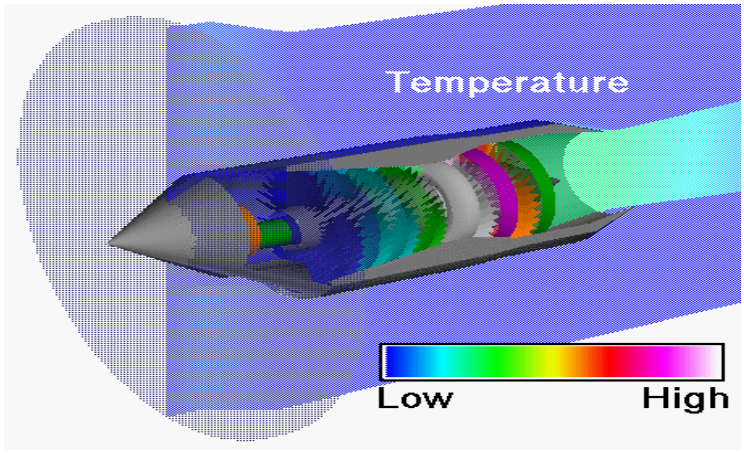

Fig. 4 - Temperature field distribution in Turboprop [2]

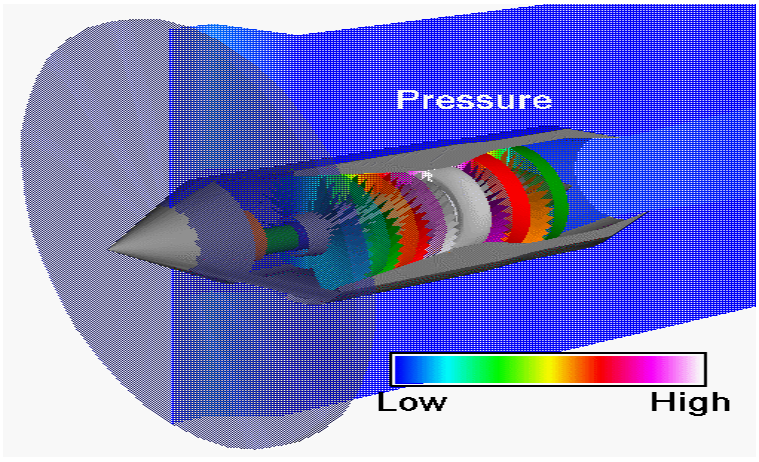

Fig. 5 - Pressure field distribution in Turboprop [2]

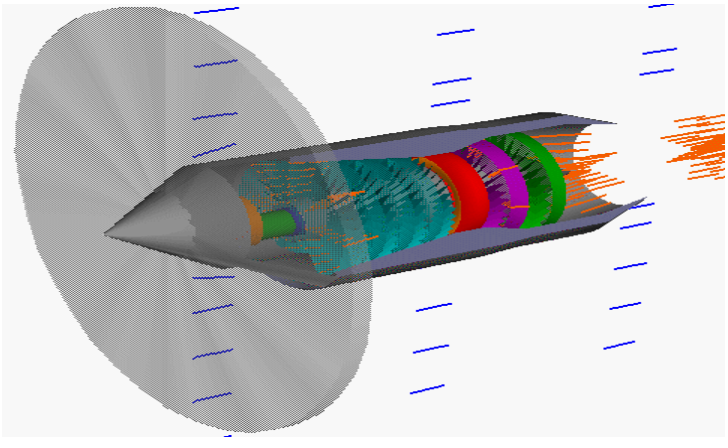

Fig. 6 - Flow field distribution in Turboprop [2]

The flow through modern axial compressors systems is highly complex. The flow is 3D and unsteady due to the relative motion between the successive blade rows and the

occurence of the viscous effects within each row. The flow is also transonic where there regions of subsonic and supersonic flow coexist. Supersonic flow generally appears near the rotor tip leading edge, usually for large diameter blades, where the highest rotational velocities are combined with the axial flow velocities, and the relative Mach number frequently exceeds the unity.

3. NUMERICAL SIMULATION AND CONCLUSIONS

The fluid flow path of an axial compressor system is convergent, with the meaning that the cross-sectional area in the direction of flow decreases. The area is diminished proportionally with the increased density of the air, as the compression progresses from stage to stage. Each stage of an axial compressor produces a small compression pressure ratio at a high efficiency, with the concern to preserve the subsonic flow regime within the compressor system. For this reason, for the high pressure ratios, the multiple staged axial flow compressors are used.

Axial compressors are also more compact, have a smaller cross section and provide higher values for the pressure ratio, in comparison with the centrifugal compressor, which are the most important advantages.

For running with the best efficiency, the compressor system must operate at constant axial velocity.

At high pressure ratios, a single staged axial compressor does not work efficiently, in comparison with multiple staged axial compressor.

When running the engine from lower speeds up to higher speeds, in case of multiple-staged axial flow compressors, operating with high values of the pressure ratio, the design of the engine must be of twin-spool or triple-spool type.

In order to achieve more flexibility and a more uniform loading of each axial compressor stage, the twin spool or triple spool construction with two or three different rotational speeds is generally used in high pressure ratio axial compressor systems.

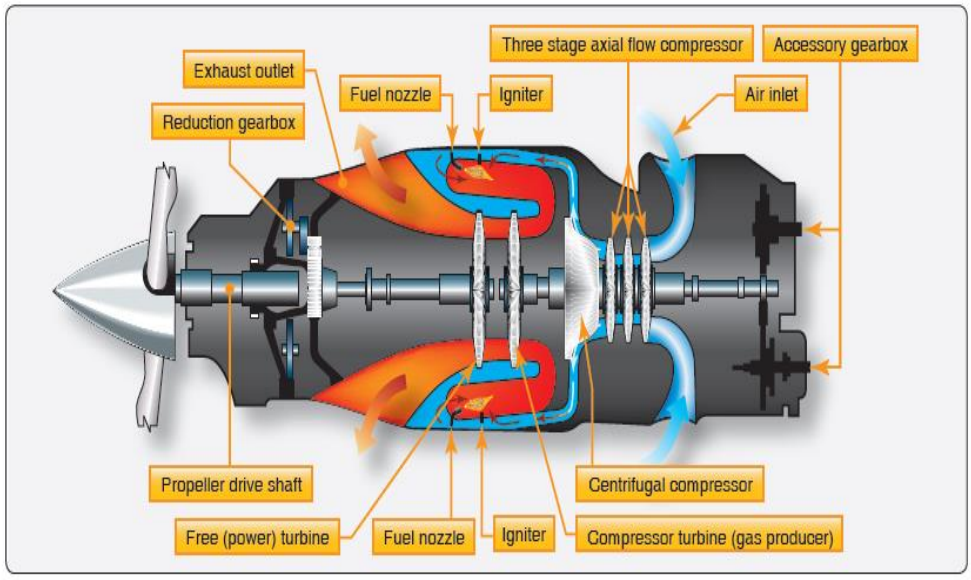

Fig. 7 - Three staged axial flow compressor [8]

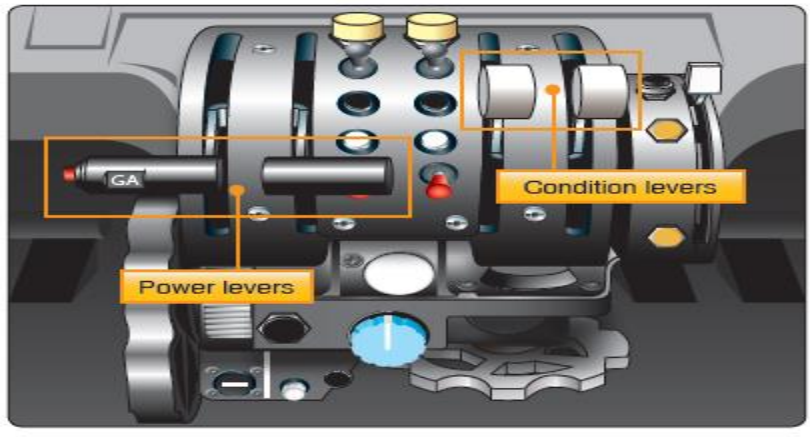

Fig. 8 - Powerplant engine control [8]

Fig. 9 - Engine instruments [8]

In order to improve the performances of the axial compressor system, with the referrence to significantly reduce the pressure losses due to shock waves and boundary layer separation, the design of the blade row cascades can be modified by the use of the sweep effect, which eventually lead to diminish of the flow velocity at tip blad, from supersonic to subsonic, such that to prevent the occurence of the shock waves at tip blade.

The numerical simulations of the flow through the transonic first rotor blade test case, have been performed for the basic reference blade, shown in Fig. 10, and the sweep effect has been investigated for the swept blades, shown in Fig. 11.

The mathematical model is based on the RANS equations; following the numerical simulations using the ANSYS FLUENT CFD code, the flow parameters have been determined.

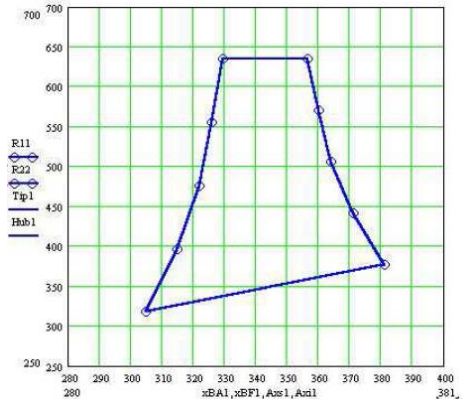

Blade view from hub to tip

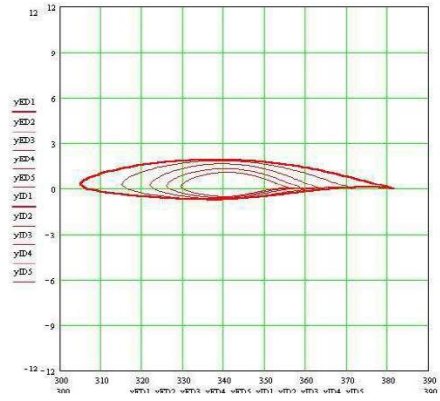

Airfoil overlap – cross section in rotor blade

Fig. 10 - Test Case - NASA Blade from the rotor first stage of a multistaged axial flow compressor

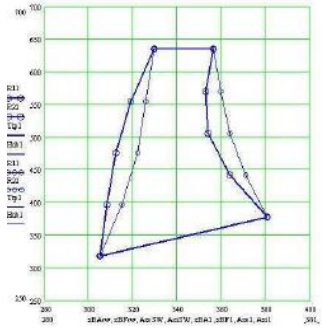

Sweep angle [deg], from hub to tip: (0,5,7,5,0)

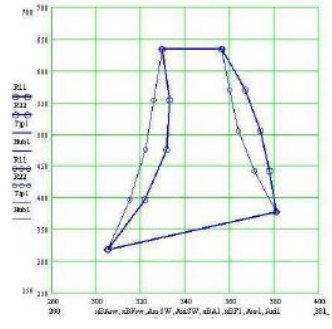

Sweep angle [deg], from hub to tip: (0,-5,-7,-5,0)

Fig. 11 - Swept blade versus basic blade

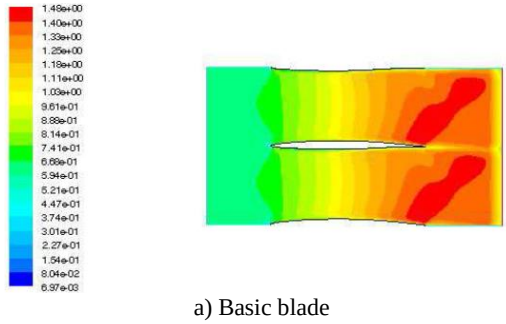

a) Basic blade

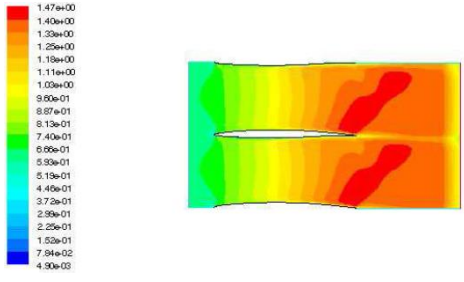

b) Forward swept blade (sweep angle =7 [deg])

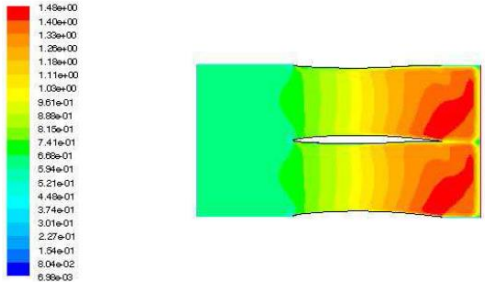

c) Backward swept blade (sweep angle = - 7 [deg])

Fig. 12 - Contours of the relative Mach number, at mid section

The airfoils at mid section have been considered for the 2D flow numerical analysis. The effect of sweep has been highlighted by the cases: forward sweep, with the sweep angle being considered 7 [deg], and backward sweep, with the sweep angle = - 7 [deg].
Fig. 12 illustrates the contours of relative mach number.

REFERENCES

[1] http://airspot.ru/book/file/485/166837_EB161_rolls_royce_the_jet_engine_fifth_edition_gazoturbinnyy_.pdf
[2] * * * https://www.grc.nasa.gov/www/k-12/airplane/ turbtyp/etph.html.
[3] * * * http://citeseerx.ist.psu.edu/viewdoc/download_doi=10.1.1.452.7664&rep=rep1&type=pdf
[4] * * * http://math.mit.edu/~gs/cse/codes/mit18086_navierstokes.pdf.
[5] A. J. Chorin, J. E. Marsden, *A mathematical introduction to fluid mechanics* Third edition, Springer, 2000.
[6] G. Strang, *Computational Science and Engineering*, First Edition, Wellesley-Cambridge Press, 2007.
[7] * * * http://web.cecs.pdx.edu/~gerry/class/ME448/notes/pdf/convectionUpwind.pdf.
[8] * * * Airplane Flying Handbook- FAA-H-8083-3B.
[9] J. D. Mattingly, *Elements of gas turbine propulsion*, Sixth reprint, 2013. https://soaneemrana.org/onewebmedia/ELEMENTS%20OF%20GAS%20TURBINE%20PROPULTION 2.pdf
[10] D. A. Anderson, J. C. Tannehill, R. H. Pletcher, *Computational Fluid Mechanics and Heat Transfer*, 2nd Ed., McGraw-Hill, New York, 1997.
[11] C. Hirsch, *Numerical Computation of Internal and External Flows*, Vol. **I** & **II**, 1st Ed., Wiley, New York, 1988.
[12] P. L. Roe, *Some Contributions to the Modeling of Discontinuous Flows*, Large-Scale Computations in Fluid Mechanics, Edited by B.E. Engquist, S. Osher, R.C.J. Somerville, Vol. **22**, Part.2, Lectures in Applied Mathematics, ASME, Providence.
[13] Y. Liu, M. Vinokur, *Upwind Algorithms for General Thermo-Chemical Nonequilibrium Flows*, AIAA Paper 89-0201.
[14] H. P. Pulliam, J. L. Steger, Implicit Finite-Difference Simulations of Three-Dimensional Compressible Flow, *AIAA Journal*, Vol. **18**, No. 2, February 1980.
[15] P. R. Spalart, S. R. Allmaras, *A One-Equation Turbulence Model for Aerodynamic Flows*, AIAA Paper 92-0439
[16] P. G. Hill, C. R. Peterson, *Mechanics and Thermodynamics of Propulsion*, 2nd Ed., Addison Wesley, Publication Co., 1992.
[17] A. S. Ucer, P. Stow, C. Hirsch, *Thermodynamics and Fluid Mechanics of Turbomachinery*, 1985
[18] J. T. Gravdahl, O. Egeland, *Compressor Surge and Rotating Stall Modeling and Control*, Springer, 1999.
[19] Y. Ochi, *Flight Control System Design for Propulsion-Controlled Aircraft*, Proceedings of the Institute of Mechanical Engineering *Part G - Journal of Aerospace Engineering*, 2005.
[20] M. Harefors, D. G. Bates, Integrated Propulsion-based Flight Control System Design for a Civil Transport Aircraft, *International Journal of Turbo and Jet Engines*, Vol. **20**, No. 2, 2003.